Internal magnetic field in thin ZnSe epilayers

S. Ghosh, N. P. Stern, B. Maertz, and D. D. Awschalom[a)]
Center for Spintronics and Quantum Computation, University of California, Santa Barbara, California 93106

G. Xiang, M. Zhu, and N. Samarth
Department of Physics, Pennsylvania State University, University Park, Pennsylvania 16802

(Received 22 September 2006; accepted 6 November 2006; published online 15 December 2006)

Strain-induced spin splitting is observed and characterized using pump-probe Kerr rotation spectroscopy in *n*-ZnSe epilayers grown on GaAs substrates. The spin splitting energies are mapped out as a function of pump-probe separation, applied voltage, and temperature in a series of samples of varying epilayer thicknesses and compressive strain arising from epilayer-substrate lattice mismatch. The strain is independently quantified using photoluminescence and X-ray diffraction measurements. The authors observe that the magnitude of the spin splitting increases with applied voltage and temperature and is highly crystal direction dependent, vanishing along $[1\bar{1}0]$. © *2006 American Institute of Physics*. [DOI: 10.1063/1.2404600]

ZnSe has been extensively investigated in the last decade for applications in optoelectronic devices operational in the blue spectral region.[1] More recently, the potential for use of ZnSe in spintronic devices has been evidenced by the long spin coherence times (~100 ns) in *n*-ZnSe and the ability to coherently transfer spins across a heterointerface between *n*-ZnSe and GaAs.[2,3] Experiments have further demonstrated electrical generation of spins in *n*-ZnSe through both current-induced spin polarization and the spin Hall effect[4] at room temperature.

Earlier studies in strained GaAs and InGaAs (Refs. 5 and 6) have revealed a *k*-linear spin splitting which acts on spins as an internally generated magnetic field. Despite the observation of electrically generated spins, no internal magnetic fields have been measured in ZnSe epilayers of micron-scale thickness. In this letter, we investigate the presence of electrically induced internal magnetic field B_{int} in strained *n*-type ZnSe epilayers. We observe an effective B_{int} proportional to the drift velocity of electrons and note that, although the bulk inversion asymmetry spin-orbit parameter in ZnSe is almost half that in GaAs,[7] the spin-splitting energy scale is comparable. Coupled with the previous studies, this establishes the potential for developing all-electrical protocols for spin initialization and coherent manipulation in this wide band gap material.

We measure three Cl-doped *n*-type ZnSe epilayers grown by molecular beam epitaxy on semi-insulating (001) GaAs substrates. The epilayer thicknesses are 100, 150, and 300 nm with carrier densities in the range of $(4-5)\times10^{17}$ cm^{-3}. Measurements of similar samples with 1.5-μm-thick ZnSe epilayers and similar carrier concentrations show no evidence of an internal magnetic field.[4] Figure 1(a) is an optical image of a patterned sample, showing channels etched along the [110] and $[1\bar{1}0]$ directions. The channels have width $w=100$ μm, length $l=235$ μm along [110] (along $[1\bar{1}0]$, $l=350$ μm), and thickness $h=100$, 150, and 300 nm. Annealed indium contact pads at the ends of each arm allow us to independently apply an electric field E along both orthogonal directions.

Growth of ZnSe on GaAs causes in-plane compressive strain in the ZnSe film due to the small lattice mismatch between the two zinc-blende semiconductors (0.25% at 300 K).[8] X-ray diffraction (XRD) measurements have shown that although biaxial strain persists in epilayers as thick as 1.6 μm,[9] the critical thickness beyond which dislocations begin to form in the ZnSe/GaAs system is about 0.17 μm.[10] We quantify the strain in our samples using both photoluminescence (PL) and XRD measurements. Figure 1(b) shows PL at $T=50$ K for the 300 and 100 nm samples. Comparing the direct band gap of a 2 μm ZnSe epilayer with similar carrier concentration at 50 K (Ref. 11) (dashed line in the figure) with the observed PL, we notice that the PL peaks are increasingly redshifted relative to the unstrained band gap with decreasing epilayer thickness. By assuming that the PL peak occurs at the direct band gap energy, we can use the shift in the PL to estimate the in-plane strain in the samples.[12] To first order, these calculations predict compressive strain in the range from 1×10^{-3} to 3×10^{-3}, which is comparable to the values quoted in existing measurements of samples of similar thicknesses.[9] XRD measurements [Figs. 1(c) and 1(d)] show further evidence of monotonically increasing strain with decreasing epilayer thickness, again in agreement with previous studies. We do not observe any anisotropy in the strain about the [115] and $[1\bar{1}5]$ directions in any of the three samples, and the diffraction pattern about the (004) peaks is found to be invariant with rotation about the growth axis [001], implying no tilt between the substrates and the epilayers.

The samples are mounted in the variable temperature insert of a magneto-optical cryostat. The electron spin dynamics is probed with time-resolved Kerr rotation (KR) spectroscopy[13,14] in the Voigt geometry using pulses from a frequency-doubled mode-locked Ti:sapphire laser with a pulse duration ~150 fs and a repetition rate of 76 MHz. A circularly polarized pump pulse normal to the sample surface injects electrons with spins polarized along the beam propagation direction z. After a time delay Δt, the Kerr rotation angle of a linearly polarized probe pulse measures the pro-

a)Electronic mail: awsch@physics.ucsb.edu

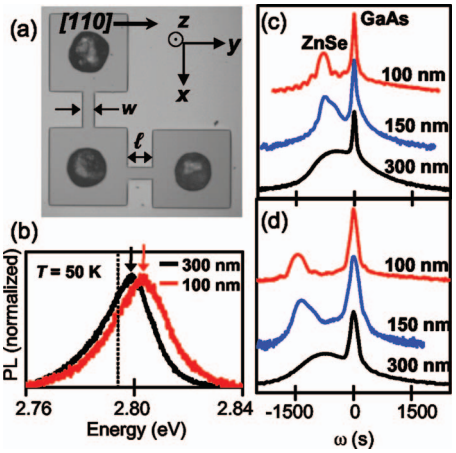

FIG. 1. (Color) (a) Optical image of processed sample showing the crystal orientation of the epilayer (l=235 μm, w=100 μm). The coordinate axes define the measurement geometry. (b) PL for 300 and 100 nm samples showing the strain-induced shift. Arrows indicate peak emission energies. Dashed line indicates the bulk, unstrained energy gap. XRD spectra for the (c) (004) and (d) (115) reflections. The appearance of interference fringes in the (004) reflection in the 100 nm sample indicates phase coherent growth and may be used to further verify the epilayer thickness.

jection of the electron spin magnetization along z as it precesses about the transverse magnetic field B_{ext} applied along y. The pump and probe energies are typically tuned in the range of 2.70–2.80 eV, to maximize the KR effect, with powers of 1 mW and 100 μW, respectively. The beams are focused to a spot size of ~20 μm, and the circular polarization of the pump beam is modulated with a photoelastic modulator at 50 kHz for lock-in detection. Time-resolved measurements[2] have shown that the electron g factor for ZnSe in these samples is 1.1.

In order to characterize the internal magnetic field B_{int}, we measure KR as a function of the applied magnetic field B_{ext} at a fixed pump-probe delay time of Δt=13 ns while varying the applied electric field E and pump-probe separation d. Figure 2(a) shows the data from the 100 nm sample (with the largest strain) at T=125 K when the pump and probe are spatially overlapped (d=0). The signal is an oscillatory function of the total magnetic field $\mathbf{B}=\mathbf{B}_{\text{ext}}+\mathbf{B}_{\text{int}}$ and is given by $A\cos(g\mu_B B\Delta t/\hbar)$,[5,6] where A is the amplitude, g the effective g factor of the sample, μ_B the Bohr magneton, and B the magnitude of the total magnetic field experienced

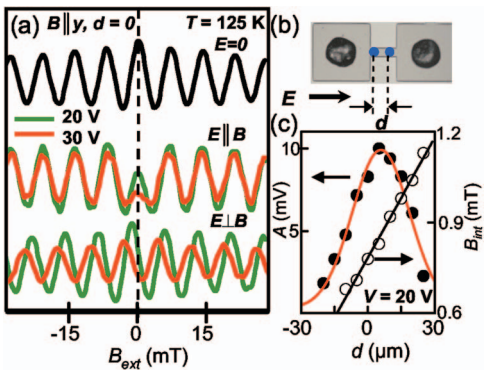

FIG. 2. (Color) Data from 100 nm sample at T=125 K. (a) Kerr rotation with pump-probe overlapped (d=0) at Δt=13 ns with (top) E=0, (center) $E\|B_{\text{ext}}$, and (bottom) $E\perp B_{\text{ext}}$. (b) Schematic of measurement geometry for spatially resolved scans. (c) A and B_{int}, obtained from fits described in the text, as a function of pump-probe separation d with $E\|B_{\text{ext}}$.

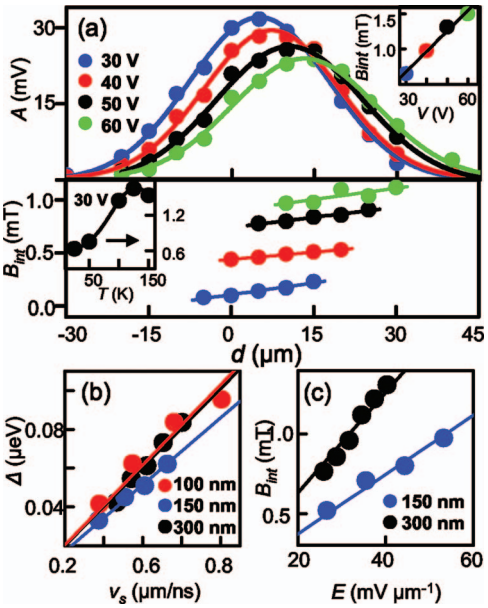

FIG. 3. (Color) (a) A and B_{int} (top and bottom) as a function of pump-probe separation d with $E\|B_{\text{ext}}$, for a series of applied voltages V at T=50 K in 100 nm sample. (Inset, top) B_{int} varies linearly with applied voltage. (Inset, bottom) B_{int} as a function of temperature T for V=20 V. Comparison of (b) electric field induced spin splitting Δ at 50 K as a function of the spin drift velocity v_s for all samples and (c) B_{int} for 300 and 150 nm samples varying with E at 50 K.

by the electrons. For KR along [110] in the absence of an applied electric field (top trace), the average k=0 and therefore B_{int}=0 and the oscillations are centered at $B=B_{\text{ext}}$=0. For E parallel to B_{ext}, the center peak is suppressed (center trace). In this geometry, B_{int} is perpendicular to B_{ext},[5,6] resulting in a total field magnitude of $B=\sqrt{B_{\text{ext}}^2+B_{\text{int}}^2}$ which is always greater than zero for a nonzero B_{int}. For larger applied voltage, B_{int} increases, resulting in greater suppression of the central peak. When the sample is rotated so that E is perpendicular to B_{ext} (bottom trace), both the external and internal magnetic fields are along y and add directly so that $B=B_{\text{ext}}+B_{\text{int}}$ and the oscillatory signal is centered at $-B_{\text{int}}$. It is noted here that all of these effects are observed in the channel along the [110] direction only. For the channel along $[1\bar{1}0]$, surprisingly no internal fields in any geometry are observed in any of the samples.

In both cases above, with nonzero electric field the amplitude of the signal decreases with increasing voltage, which is further investigated by spatially separating the pump and the probe by a distance d along the direction of E [Fig. 2(b)]. Due to the laser profile of the pump beam, the optically injected spins have a Gaussian spatial profile which is centered at d=0 μm when E=0. An applied voltage ($E\neq 0$) imparts a nonzero average momentum k to the injected spin packet, causing it to drift with an average velocity v_s. We fit the amplitude A as a function of d to determine the center position d_c=6 μm of the spin packet with applied voltage of 20 V after 13 ns, giving v_s=0.46 μm/ns. Figure 2(c) shows the spatial variation of B_{int} throughout the spin packet for E parallel to B_{ext}. Spins at the leading edge of the packet experience a larger B_{int} than the trailing edge. This variation is due to the spread in the drift velocities of the spin packet arising from spin diffusion. The reported value of B_{int} for each voltage is obtained from a linear fit at $d=d_c$.

Figure 3(a) shows both data and fits for A (top) and B_{int}

(bottom) of the spin packet as measured by KR at different applied voltages in the 100 nm sample at $T=50$ K. B_{int} increases linearly with applied voltage (inset, top) confirming the k-linear dependence. It also increases with T, almost doubling as T changes from 25 to 150 K (inset, bottom). It has been observed[15] that the in-plane biaxial strain in a 100 nm ZnSe/GaAs epilayer increases in magnitude with increasing T due to the thermal changes in the lattice and elastic constants of both epilayer and substrate, which may explain the changes observed here. However, without more systematic data on the alteration of B_{int} with strain, this remains speculative. While spin precession in these samples persists to higher temperatures, at $T>150$ K the spin lifetime is not long enough to quantify the internal field.

Figure 3(b) shows the variation of the spin-splitting energy $\Delta=g\mu_B B_{\text{int}}$ with the spin drift velocity v_s for all samples at $T=50$ K. From linear fits to the data, we use the slope $\beta=\Delta/v_s$ to characterize the samples and find $\beta=101$, 86, and 103 neV ns/μm for the 300, 150, and 100 nm samples, respectively. Previous measurements[6] in GaAs samples with strain in a similar region of $(2-3)\times10^{-3}$ have shown β values ranging between 75 and 125 neV ns/μm.

The contact resistances in the samples are non-negligible and the effective electric field across each channel cannot be simply calculated from the applied voltage. Resistivity obtained from transport measurements is used to calculate the electric field in the two thicker samples, and in Fig. 3(c) we compare B_{int} between the 300 and 150 nm samples as a function of E. Surprisingly, we observe the thicker sample, with less strain, having a larger internal magnetic field for the same electric field. Unfortunately, for the 100 nm sample the contact resistance is too large to allow any reliable estimate of the electric field.

In conclusion, we have quantitatively measured the k-linear internal magnetic field as a function of voltage in three samples. At this point we do not have a complete understanding of the correlation between the internal magnetic field and strain in ZnSe, since comparison between the 300 and 150 nm samples shows an increased spin splitting with decreasing strain. This effect is not systematic, as we do not observe any internal fields in the largely strain relaxed 1.5 -μm-thick sample. We also observe B_{int} only along the [110] direction in the samples while the strain is isotropic, which, though not well understood, may be exploited to design spin manipulation using topological effects.[16]

The authors thank NSF and ONR for financial support and H. Knotz and Y. Li for assistance with the XRD measurements. One of the authors (N.P.S.) acknowledges the support of the Fannie and John Hertz Foundation.

[1] M. A. Haase, J. Qiu, J. M. DePudyt, and H. Cheng, Appl. Phys. Lett. **59**, 1272 (1991).
[2] I. Malajovich, J. M. Kikkawa, J. J. Berry, N. Samarth, and D. D. Awschalom, Phys. Rev. Lett. **84**, 1015 (2000).
[3] I. Malajovich, J. J. Berry, N. Samarth, and D. D. Awschalom, Nature (London) **411**, 770 (2001).
[4] N. P. Stern, S. Ghosh, G. Xiang, M. Zhu, N. Samarth, and D. D. Awschalom, Phys. Rev. Lett. **97**, 126603 (2006).
[5] Y. Kato, R. C. Myers, A. C. Gossard, and D. D. Awschalom, Nature (London) **427**, 50 (2004).
[6] V. Sih, H. Knotz, J. Stephens, V. R. Horowitz, A. C. Gossard, and D. D. Awschalom, Phys. Rev. B **73**, 241315(R) (2006).
[7] R. Winkler, *Spin-Orbit Coupling Effects in Two-Dimensional Elecron and Hole Systems* (Springer, New York, 2003), 27, Chap. 3.4.
[8] O. Madelung, *Semiconductors: Data Handbook* (Springer, New York, 2003), pp. 120 and 210.
[9] A. G. Kontos, E. Anastassakis, N. Chrysanthakopoulos, M. Calamiotou, and U. W. Pohl, J. Appl. Phys. **86**, 412 (1999).
[10] K. Ohkawa, T. Mitsuyu, and O. Yamazaki, Phys. Rev. B **38**, 12465 (1998).
[11] S. Z. Wang, S. F. Yoon, L. He, and X. C. Shen, J. Appl. Phys. **90**, 2314 (2001).
[12] K. Mohammed, D. A. Cammack, R. Dalby, P. Newbury, B. L. Greenberg, J. Petruzello, and R. N. Bhargava, Appl. Phys. Lett. **50**, 37 (1986).
[13] S. A. Crooker, D. D. Awschalom, J. J. Baumberg, F. Flack, and N. Samarth, Phys. Rev. B **56**, 7574 (1997).
[14] S. A. Crooker, D. D. Awschalom, and N. Samarth, IEEE J. Sel. Top. Quantum Electron. **1**, 1082 (1995).
[15] R. J. Thomas, B. Rockwell, H. R. Chandrasekhar, M. Chandrasekhar, A. K. Ramdas, M. Kobayashi, and R. L. Gunshor, J. Appl. Phys. **78**, 6569 (1995).
[16] Y. K. Kato, R. C. Myers, A. C. Gossard, and D. D. Awschalom, Appl. Phys. Lett. **87**, 022503 (2005).